Solid-State Electronics 199 (2023) 108495

Contents lists available at ScienceDirect

Solid State Electronics

journal homepage: www.elsevier.com/locate/sse

New insights into the effect of spatially distributed polarization in ferroelectric FET on content addressable memory operation for machine learning applications

Chang Su [a], Weikai Xu [a], Lining Zhang [b,c], Ru Huang [a,c,d], Qianqian Huang [a,c,d,*]

[a] School of Integrated Circuits, Peking University, Beijing 100871, China
[b] School of Electronic and Computer Engineering, Peking University, Shenzhen 518055, China
[c] Beijing Advanced Innovation Center for Integrated Circuits, Beijing 100871, China
[d] Chinese Institute for Brain Research, Beijing 102206, China

ARTICLE INFO

The review of this paper was arranged by "Francisco Gamiz"

Keywords:
TCAD simulation
FeFET
CAM

ABSTRACT

In this work, the impacts of spatially distributed polarization in Ferroelectric FET (FeFET) on the performance of content addressable memory (CAM) circuits are investigated. It is found that for CAM operation with large pre-charging voltage in the match line, the storage state in FeFET will be changed with the lower polarization near drain side, resulting in the strong non-uniformity of polarization along the channel direction. The lateral electric field generated by source and drain junction due to short channel effect will further exacerbate this effect. It is further shown that this distributed polarization effect may lead to significant circuit performance difference compared with uniform polarization situation, and may further degrade the search accuracy especially for multi-bit CAM. This work indicates the crucial role of polarization distribution effect in the device-circuit co-optimization of FeFET.

1. Introduction

Content addressable memory (CAM) has drawn significant interests for data-centric machine learning (ML) applications due to its high parallel pattern matching capability [1,2], while conventional SRAM-based CAM suffers from large area overhead [3]. Therefore, various emerging non-volatile memories (NVM) have been applied to implement more compact cells [4–6]. Among them, HfO_2-based FeFET Ternary CAM (TCAM) can significantly boost the CAM density due to ultra-compact structure [6], with additional advantages of large on–off ratio, low write energy [2] and high CMOS compatibility [7–9]. As shown in Fig. 1(a) and (b), the pre-charged high voltage of match line (ML) would be maintained only when both of two parallel FeFETs with distinct threshold values are turned-off under the corresponding search line (SL) voltage, which represents the match condition between stored data and search data. Moreover, the multi-level states caused by partial polarization switching of ferroelectric (FE) enable the realization of FeFET-based multi-bit CAM (MCAM) design [10,11].

To evaluate the FeFET-based CAM circuit performance, the accurate FeFET device model is of great importance. The prevailing FeFET models [12,13] are usually established by directly solving the FE model with baseline MOSFET model, which are intrinsically a lumped treatment for FeFET with internal metal layer structure [14]. However, for FeFET without an internal metal layer in the gate stack, the polarization (P_{FE}) and the FE voltage (V_{FE}) may vary spatially in the longitudinal direction at a nonzero drain bias as shown in Fig. 1(c), and can also be influenced by the lateral electric field at drain or source edges [15]. Therefore, the polarization distributed along the channel direction of FeFET without internal metal layer is non-uniform, which may directly impact the device channel conduction and the FeFET-based CAM circuit performance. It is noted that this phenomenon is an intrinsic issue caused by the device structure, instead of causing by variation sources in FeFET explored by multiple research groups [16–19].

In this work, for the first time, the impact of distributed polarization in FeFET on the CAM circuit performance is investigated by simulation. Different from the FeFET with uniform polarization, the device with polarization distribution effect shows the significantly different conduction capability considering the high drain bias especially in the multi-bit CAM applications, indicating its crucial role in the device-circuit co-optimization of FeFET.

* Corresponding author.
E-mail addresses: ruhuang@pku.edu.cn (R. Huang), hqq@pku.edu.cn (Q. Huang).

https://doi.org/10.1016/j.sse.2022.108495

Available online 26 October 2022
0038-1101/© 2022 Elsevier Ltd. All rights reserved.

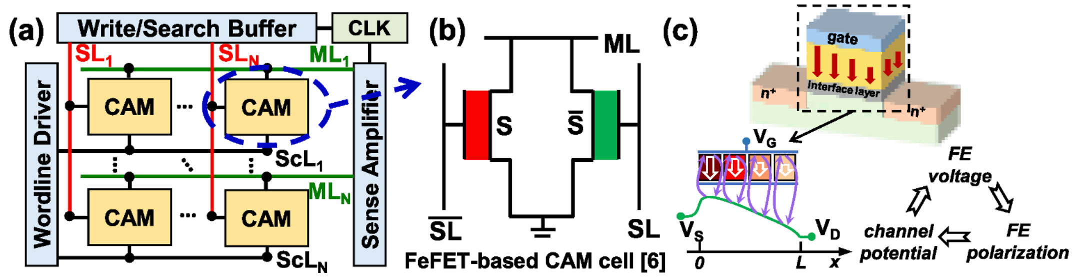

Fig. 1. (a) Architecture of the CAM array. (b) The basic structure of 2FeFET-based CAM cell [6]. (c) The schematic of FeFET with spatially distributed polarization.

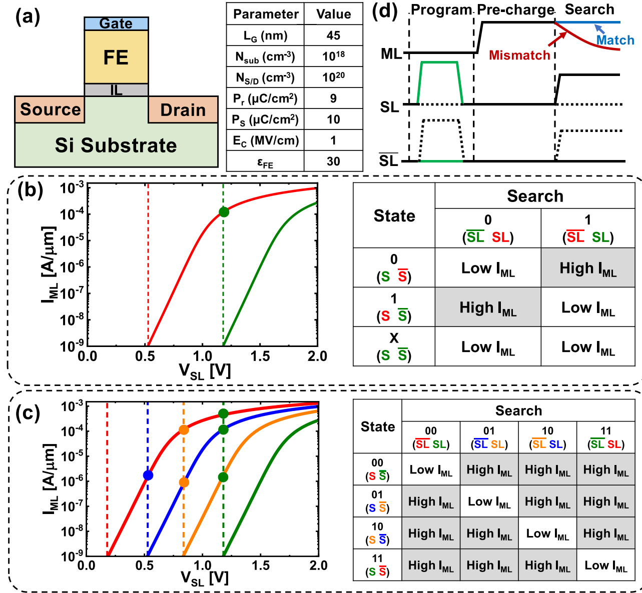

Fig. 2. (a) Schematic structure of the FeFET simulated in this work with FE parameters referred to [22]. Simulated I_D-V_G curves and truth table for (b) TCAM and (c) MCAM. The transfer curves show different threshold voltages due to different polarization states, which are programmed by gate voltage pulses with the same width and different amplitudes. (d) The waveform of operation voltage in CAM application.

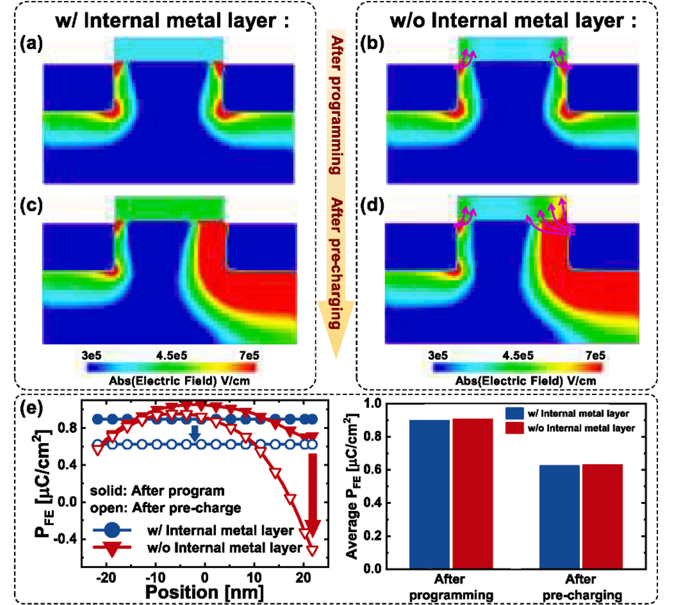

Fig. 3. (a)–(d) Electric field contours for bulk FeFET w/ and w/o internal metal layer after programming and pre-charging respectively with gate voltage of zero. For programming operation, the voltage of gate and drain are 3.5 V and 0 V respectively. For pre-charging operation, the voltage of gate and drain are 0 V and 1.2 V respectively. Besides, the voltage of source and bulk are always zero for both operations. (e) P_{FE} distribution along the channel and the corresponding average value after programming and pre-charging with gate voltage of zero.

2. Simulation Method

To investigate the impact of distributed polarization on the CAM cell, the mixed mode simulation in Sentaurus TCAD [20] is carried out. For the simulation of FeFET, the schematic structure is shown in Fig. 2(a), where the gate stack is composed of a 10 nm-thick FE-HfO_2 layer and a 1.2 nm-thick interfacial layer of AlON [21]. The basic structure parameters are listed in Fig. 2(a), in which the FE parameters refer to [22], where the chosen value of P_r is low to improve reliablity and memory window (MW) of FeFET [23]. The Preisach model [24] is utilized to describe polarization switching. Besides, the physical models for transistor include doping-dependent model, thin layer model and high-field saturation model for mobility, the Shockley-Read-Hall model and Auger model for recombination and old Slotboom model for bandgap narrowing.

For the simulation of CAM cell, different polarization states are programmed by the same-width pulses of gate voltage (V_G) with different amplitudes at first, the corresponding I_D-V_G curves are plotted in Fig. 2(b) and (c). Then the ML is pre-charged to the voltage equal to VDD. In the searching phase, the relatively small V_G with the related amplitudes (V_{SL}) are subsequently applied according to the search query. The truth table of TCAM and 2-bit MCAM are listed in Fig. 2(b) and (c). As shown in Fig. 2(d), the operation results of the CAM cell are dependent on the discharging speed of ML voltage (V_{ML}) during the search phase, which is directly decided by the conduction current (I_{ML}) of the parallel FeFET.

3. Results and discussion

3.1. A. The spatially distributed polarization in FeFET

To investigate the P_{FE} distribution effect, FeFET with an internal metal layer is also simulated for comparison, which is also consistent with the results by utilizing the currently modeling method of FeFET for CAM design. Fig. 3(a) and (b) show the electric field contours after program voltage pulse for FeFET with and without an internal metal layer. It can be seen that in both devices, channel electric field spatially distributes along the channel direction, which is resulted from the impacts of source/drain (S/D) depletion regions [25]. For the FeFET with an internal metal layer, due to the role of equipotential layer played by the internal metal layer, the distribution of electric field in FE is uniform along the channel direction as shown in Fig. 3(a). However, for FeFET without internal metal layer as shown in Fig. 3(b), electric field in FE is directly influenced by the channel electric field, which is non-uniform

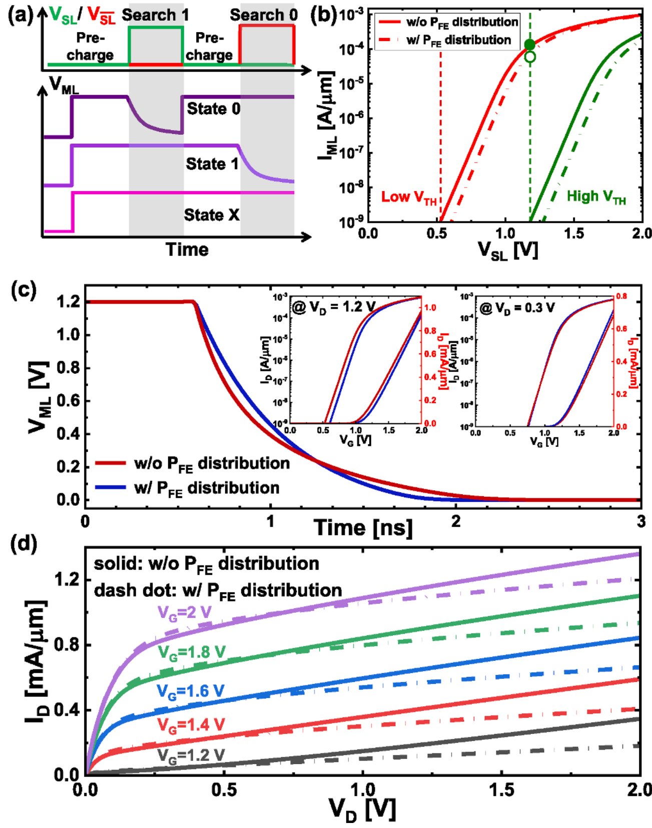

Fig. 4. (a) Search operation of TCAM. (b) The impacted I_D-V_G curves due to the distributed P_{FE}. The V_{SL} of FeFET are represented by the dashed vertical lines. Different (c) discharging process and (d) I_D-V_D caused by the P_{FE} distribution.

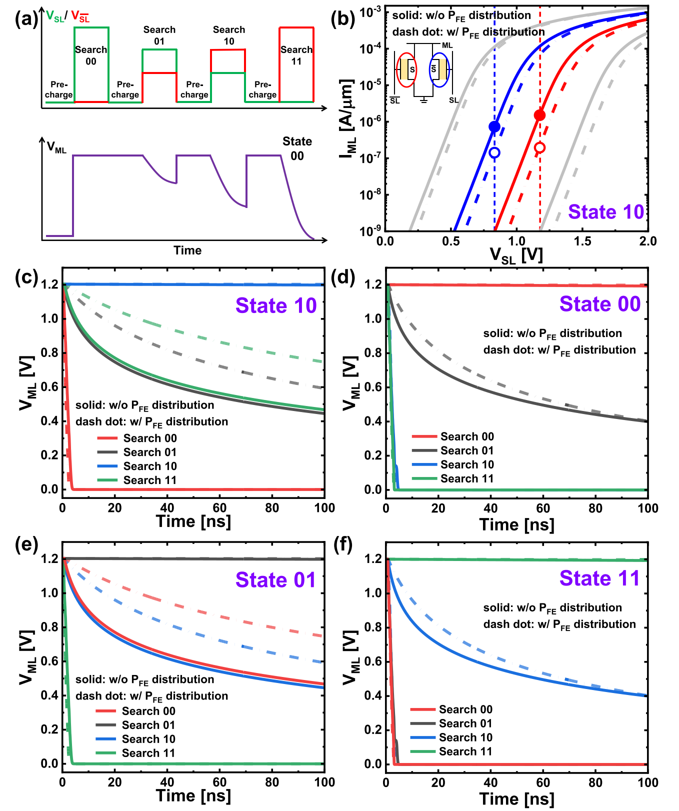

Fig. 5. (a) Search operation of 2-bit MCAM. (b) For storage state "10", the impacted I_D-V_G curves due to the distributed P_{FE}. The V_{SL} of the discharging FeFET when searching state "01" and state "11" are represented by the dashed vertical lines with blue and red respectively. The corresponding discharging FeFET devices are circled in the inset respectively. Different discharging process caused by the P_{FE} distribution for (c) state "10", (d) state "00", (e) state "01" and (f) state "11".

along the channel. Moreover, it can be noticed that the participation of lateral electric field generated by S/D junction with the vertical field in FE gradually decreases from S/D edge to the center of channel.

Moreover, considering the special operation of CAM, a high drain bias (V_D or V_{ML}) of 1.2 V would be applied during the pre-charging phase. As shown in Fig. 3(c) and (d), the non-uniformity of electric field in channel becomes stronger. As shown in Fig. 3(d), since the impact of high drain bias is stronger near the drain region, the corresponding change of electric field in FE increases near the drain region, leading to the spatially distributed P_{FE}.

Fig. 3(e) shows the P_{FE} distribution of above two devices after program and pre-charge phase. Considering the situation that the duration of pre-charge phase is sufficiently long, after programming, P_{FE} of FeFET without internal metal layer is spatially non-uniform distributed. The stronger depolarization field caused by lateral electric field from S/D junction [15] leads to the lower P_{FE} locally. During pre-charging phase, depolarization field near drain region increases, and thus the related P_{FE} decreases. However, for FeFET with internal metal layer, the electric field in FE is always uniform, leading to the same P_{FE} distributed along the channel direction without considering variation sources in FE layer.

3.2. Impact of spatially distributed P_{FE} on FeFET TCAM

Based on the discussion of spatially distributed P_{FE} in FeFET, its impacts on CAM circuit are evaluated. The schematic of search operation for TCAM is shown in Fig. 4(a), where the discharge process will directly influence the final results. Fig. 4(b) shows the transfer characteristics after pre-charging phase with V_{ML} of VDD. It can be seen that with P_{FE} distribution, the I_{ML} is lower, indicating the slower discharging speed during search phase. Fig. 4(c) shows the complete discharge process of TCAM for mismatch condition. It can be noticed that there is an intersect between the V_{ML} of two different FeFET devices. At the beginning of search phase with relatively large V_{ML}, V_{ML} of FeFET with P_{FE} distribution decreases much slower due to the smaller I_{ML} as shown in the inset of Fig. 4(c). With the evolution of discharging, V_{ML} gradually decreases and the I_{ML} of FeFET with P_{FE} distribution becomes the higher one. Additionally, the difference of discharging process will be more significant with the smaller MW.

To further analyze the I_{ML} difference after pre-charging phase, the I_D-V_D curves of FeFET devices are simulated with various V_G under relatively fast V_D sweep to avoid extra P_{FE} back-switching, as shown in Fig. 4 (d). For low V_D, the I_{ML} difference is negligible. This is because that the channel conduction is mainly modulated by average P_{FE}. According to Fig. 3(e), although the P_{FE} non-uniformly distributes in FeFET without internal metal layer, the average P_{FE} across FE layer is approximately the same to that of FeFET with internal metal layer. The slight current difference with low V_D implies that the prevailing model method of FeFET is reasonable and applicable for memory applications. However, for high V_D, the I_{ML} difference is distinct. Due to the increased effect of drain-channel coupling, the channel conduction is directly dependent on the region near drain junction. Based on the discussion in part A, the P_{FE} near the drain region is lower for FeFET without internal metal layer, leading to the obviously lower I_{ML}, which indicates the necessity of device-circuit co-optimization considering P_{FE} distribution effect for CAM application.

3.3. Impact of spatially distributed P_{FE} on FeFET MCAM

Furthermore, the P_{FE} distribution impact is investigated for MCAM

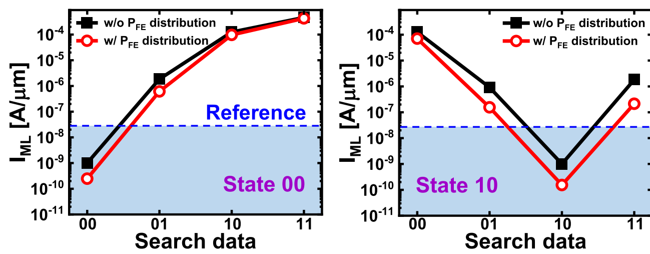

Fig. 6. For a 2-bit MCAM, a complete comparison of I_{ML} between the devices with and without the P_{FE} distribution effect.

application. To simplify the discussion, a 2-bit MCAM cell is evaluated, where the schematic of search operation is plotted in Fig. 5(a). As shown in Fig. 5(b), for intermediate state with partially switched P_{FE}, the I_{ML} difference is significant under the same V_{SL}, which can be approximately an order of magnitude due to the P_{FE} distribution effect. The different channel conduction will directly influence the discharging process, leading to the deviated search results. According to the truth table as shown in Fig. 2(c), to comprehensively evaluate the impact of P_{FE} distribution, the search operation for state "10" and "00" are simulated at first, which represent different threshold values caused by different switched P_{FE}. Compared Fig. 5(c) with Fig. 5(d), due to the more distinct I_{ML} difference for intermediate state, the difference of discharging process for state "10" is more significant. Besides, owing to the much lower I_{ML} of FeFET with P_{FE} distribution, when searching "01" and "11" for state "10", an obvious degradation of search delay is observed. Especially for searching "11", when the search time is limited, the final result might be identified as match condition mistakenly. Then the search operation for the rest storage states, including "01" and "11", are plotted in Fig. 5(e) and (f), further indicating the distinct impact of P_{FE} distribution for intermediate storage state "01". Hence, the search accuracy of CAM will be reduced due to the significant search delay.

Moreover, the comparison of ML discharging current between FeFET with and without P_{FE} distribution effect for a 2-bit MCAM is shown in Fig. 6. Due to the similarity between the results for storage state "00" and state "11", storage state "10" and state "01", only the I_{ML} comparison for state "00" and "10" are plotted. It is demonstrated that the evaluation of FeFET-based CAM by the prevailing modeling method will lead to the severe deviation for intermediate state.

4. Conclusion

This work simulates and investigates the impacts of spatially distributed polarization on the performance of FeFET-based CAM. Compared with the uniform polarization situation, the P_{FE} distribution may induce the larger V_{TH} and smaller current under a high drain bias in FeFET. For CAM operations with relatively larger drain bias than the conventional memory applications, the P_{FE} distribution will lead to significant difference in circuit performance, showing its crucial role in the device-circuit co-optimization.

Declaration of Competing Interest

The authors declare that they have no known competing financial interests or personal relationships that could have appeared to influence the work reported in this paper.

Data availability

Data will be made available on request.

Acknowledgements

This work was supported by National Key R&D Program of China (2018YFB2202801), NSFC (61927901), Beijing Nova Program of Science and Technology (Z191100001119101), BJSAMT Project (SAMT-BD-KT-22030101) and 111 Project (B18001).

References

[1] Graves CE, Li C, Sheng X, Miller D, Ignowski J, Kiyama L, et al. In-memory computing with memristor content addressable memories for pattern matching. Adv Mater 2020;32(37):2003437.
[2] Ni K, Yin X, Laguna AF, Joshi S, Dünkel S, Trentzsch M, et al. Ferroelectric ternary content-addressable memory for one-shot learning. Nat Electron 2019;2(11):521–9.
[3] Pagiamtzis K, Sheikholeslami A. Content-addressable memory (CAM) circuits and architectures: a tutorial and survey. IEEE J Solid-State Circuits 2006;41(3):712–7. https://doi.org/10.1109/JSSC.2005.864128.
[4] Li J, Montoye RK, Ishii M, Chang L. 1 Mb 0.41 μm^2 2T–2R cell nonvolatile TCAM with two-bit encoding and clocked self-referenced sensing. IEEE J Solid-State Circuits 2014;49(4):896–907. https://doi.org/10.1109/JSSC.2013.2292055.
[5] Li C, Graves CE, Sheng X, Miller D, Foltin M, Pedretti G, et al. Analog content-addressable memories with memristors. Nat Commun 2020;11(1):1638. https://doi.org/10.1038/s41467-020-15254-4.
[6] Yin X, Ni K, Reis D, Datta S, Niemier M, Hu XS. An ultra-dense 2FeFET TCAM design based on a multi-domain FeFET model. IEEE Trans Circuits Syst II Express Briefs 2019;66(9):1577–81. https://doi.org/10.1109/TCSII.2018.2889225.
[7] Park MH, Kim HJ, Kim YJ, Lee W, Moon T, Hwang CS. Evolution of phases and ferroelectric properties of thin $Hf_{0.5}Zr_{0.5}O_2$ films according to the thickness and annealing temperature. Appl Phys Lett 2013;102(4):242905. https://doi.org/10.1063/1.4811483.
[8] Xiao W, Peng Y, Liu Y, Duan H, Bai H, Yu B, et al. $Hf_{0.5}Zr_{0.5}O_2$ 1T–1C FeRAM arrays with excellent endurance performance for embedded memory. Sci China Inf Sci 2022; Accepted, https://doi.org/10.1007/s11432-022-3469-5.
[9] Yang M, Huang Q, Wang K, Su C, Chen L, Wang Y, et al. Physical investigation of subthreshold swing degradation behavior in negative capacitance FET. Sci China Inf Sci 2022;65(6):169402. https://doi.org/10.1007/s11432-021-3283-5.
[10] Yin X, Li C, Huang Q, Zhang Li, Niemier M, Hu XS, et al. FeCAM: a universal compact digital and analog content addressable memory using ferroelectric. IEEE Trans Electron Devices 2020;67(7):2785–92.
[11] Kazemi K, Sharifi MM, Laguna AF, Muller F, Rajaei R, Olivo R, et al. In-Memory Nearest Neighbor Search with FeFET Multi-Bit Content-Addressable Memories. 2021 Design, Automation & Test in Europe Conference & Exhibition (DATE) 20201;1084-9. https://doi.org/10.23919/DATE51398.2021.9474025.
[12] Ni K, Jerry M, Smith JA, Datta S. A circuit compatible accurate compact model for ferroelectric-FETs. IEEE Symposium on VLSI Technology 2018;2018:131–2. https://doi.org/10.1109/VLSIT.2018.8510622.
[13] Deng S, Yin G, Chakraborty W, Dutta S, Datta S, Li X, et al. A comprehensive model for ferroelectric FET capturing the key behaviors: scalability, variation, stochasticity, and accumulation. IEEE Sympos VLSI Technol 2020;2020:1–2. https://doi.org/10.1109/VLSITechnology18217.2020.9265014.
[14] Duarte JP, Khandelwal S, Khan AI, Sachid A, Lin Y-K, Chang H-L, et al. Compact models of negative-capacitance FinFETs: Lumped and distributed charge models. 2016 IEEE International Electron Devices Meeting (IEDM) 2016;30.5.1-4. https://doi.org/10.1109/IEDM.2016.7838514.
[15] Jindal S, Manhas SK, Gautam SK, Balatti S, Kumar A, Pakala M. Investigation of gate-length scaling of ferroelectric FET. IEEE Trans Electron Devices 2021;68(3):1364–8. https://doi.org/10.1109/TED.2021.3054720.
[16] Yin X, Müller F, Huang Q, Li C, Imani M, Yang Z, et al. An Ultra-Compact Single FeFET Binary and Multi-Bit Associative Search Engine. arXiv 2022. https://doi.org/10.48550/arXiv.2203.07948.
[17] Liu YS, Su P. Variability analysis for ferroelectric FET nonvolatile memories considering random ferroelectric-dielectric phase distribution. IEEE Electron Device Lett 2020;41(3):369–72. https://doi.org/10.1109/LED.2020.2967423.
[18] Garg C, Chauhan N, Deng S, Khan AI, Dasgupta S, Bulusu A, et al. Impact of random spatial fluctuation in non-uniform crystalline phases on the device variation of ferroelectric FET. IEEE Electron Device Lett 2021;42(8):1160–3.
[19] Xiang Y, Bardon M. G, Kaczer B, Alam Md N. K, Ragnarsson L.-Å, Groeseneken G, et al. Implication of Channel Percolation in Ferroelectric FETs for Threshold Voltage Shift Modeling. 2020 IEEE International Electron Devices Meeting (IEDM) 2020;18.2.1-4. https://doi.org/10.1109/IEDM13553.2020.9371907.
[20] Sentaurus Device User Guide Version: O-2018.06, Synopsys, Mountain View, CA, USA, June. 2018.
[21] Chan C-Y, Chen K-Y, Peng HK, Wu Y-H. FeFET memory featuring large memory window and robust endurance of long-pulse cycling by interface engineering using high-k AlON. IEEE Sympos VLSI Technol 2020;2020:1–2. https://doi.org/10.1109/VLSITechnology18217.2020.9265103.
[22] Muller J, Polakowski P, Muller S, Mulaosmanovic H, Ocker J, Mikolajick T. High endurance strategies for hafnium oxide based ferroelectric field effect transistor. 2016 16th Non-Volatile Memory Technology Symposium (NVMTS) 2016; 1-7. https://doi.org/10.1109/NVMTS.2016.7781517.

[23] Pahwa G, Salahuddin S, Hu C. Critical importance of nonuniform polarization and fringe field effects for scaled ferroelectric FinFET memory. IEEE Trans Electron Devices 2022;69(9):4900–8. https://doi.org/10.1109/TED.2022.3190252.

[24] Jiang B, Zurcher P, Jones RE, Gillespie SJ, Lee JC. Computationally Efficient Ferroelectric Capacitor Model For Circuit Simulation. 1997 Symposium on VLSI Technology 1997; 141-142. https://doi.org/10.1109/VLSIT.1997.623738.

[25] Saha AK, Sharma P, Dabo I, Datta S, Gupta SK. Ferroelectric transistor model based on self-consistent solution of 2D Poisson's, non-equilibrium Green's function and multi-domain Landau Khalatnikov equations. 2017 IEEE International Electron Devices Meeting (IEDM) 2017;13.5.1-4. https://doi.org/10.1109/IEDM.2017.8268385.